Journal of Computer and Communications, 2026, 14(1), 136-144
https://www.scirp.org/journal/jcc
ISSN Online: 2327-5227
ISSN Print: 2327-5219

# Broadband Polarization Conversion Transmissive Janus Metasurface

**Wenxin Liu, Hexiu Xu***

Anti-Air and Anti-Missile Academy, Air Force Engineering University, Xi'an, China
Email: *838583594@qq.com

**How to cite this paper:** Liu, W.X. and Xu, H.X. (2026) Broadband Polarization Conversion Transmissive Janus Metasurface. *Journal of Computer and Communications*, **14**, 136-144.
https://doi.org/10.4236/jcc.2026.141008

**Received:** December 18, 2025
**Accepted:** January 27, 2026
**Published:** January 30, 2026

## Abstract

This study addresses the limitations of conventional metasurfaces, which exhibit symmetric electromagnetic responses under forward and backward incidences and are difficult to achieve distinct functionalities and wavefront control. A multi-layer metasurface based on a polarization-ordered binary double-sided design is proposed. By breaking spatial symmetry at the structural level, diode-like asymmetric transmission and independent wavefront control are achieved. The design adopts a checkerboard-like staggered arrangement of unit cells, enabling different functionalities under forward and backward incidences for the same polarized wave. Orthogonal polarization conversion and broadband phase coverage are realized using multi-layer twisted metallic structures and a grating layer. Simulation results demonstrate that the metasurface achieves a −30˚ beam deflection under forward incidence, while generating a vortex beam with topological charge 1 under backward incidence. The two channels exhibit good isolation, along with broadband and high transmission efficiency characteristics. This research provides new insights for high-performance non-reciprocal devices, bidirectional multifunctional integrated antennas, and information-encryption surfaces.

## Keywords

Metasurfaces, Janus, Broadband

## 1. Introduction

As an artificial two-dimensional material composed of subwavelength elements, metasurfaces have demonstrated significant potential in recent years across fields such as beamforming [1], polarization control [2], stealth [3]-[5], and Multifunctional integration [6], owing to their exceptional ability to control electromagnetic waves. Most traditional transmissive metasurfaces are designed based on spatially

symmetric elements, and their electromagnetic responses generally satisfy the reciprocity theorem, resulting in identical control effects for forward and backward incident waves. This makes it difficult to achieve asymmetric transmission and dual-sided independent imaging functionalities. However, in unidirectional transmission devices, electromagnetic isolation, information encryption, and bidirectional multifunctional antenna systems, there is often a need for differentiated wavefront control of incident waves from different directions or frequencies within the same aperture. This imposes urgent requirements for the non-reciprocal design and functional integration of metasurfaces. Although Janus metasurfaces [7]-[9] have been developed in recent years, most of them exhibit narrow frequency ranges and primarily rely on bit-wise phase control.

To address the aforementioned challenges, this paper proposes a multi-layer metasurface based on a polarization-ordered binary double-sided imaging design. By breaking spatial symmetry at the element level and adopting a checkerboard staggered arrangement at the system level, the design achieves diode-like asymmetric transmission effects under forward and backward incidences. Furthermore, it realizes beam deflection in the forward direction and vortex beam generation in the backward direction, as shown in **Figure 1**. This design not only enriches the implementation methods for double-sided imaging metasurfaces but also provides novel device solutions for shared-aperture multifunctional antennas, dynamic information encryption surfaces, and intelligent stealth technologies.

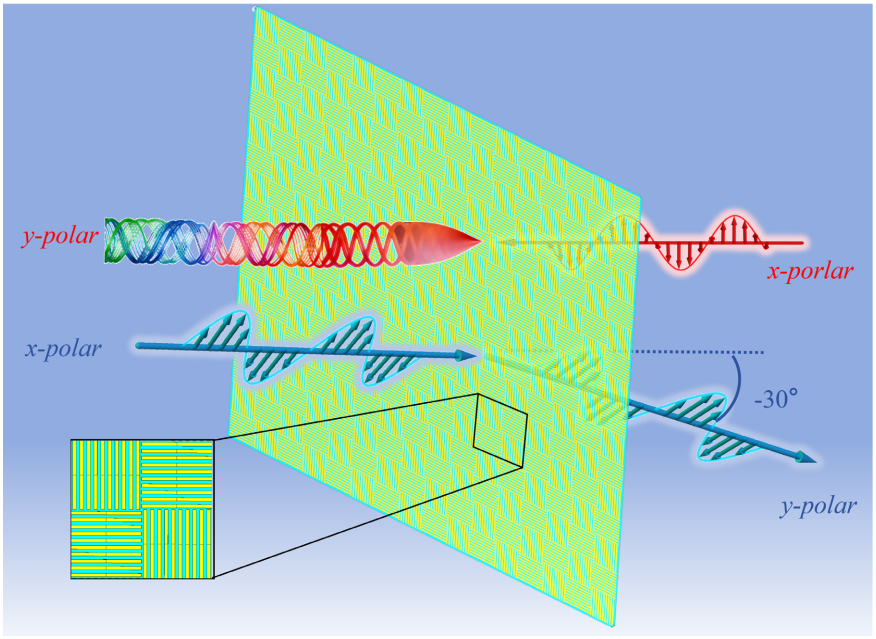


**Figure 1.** Functional schematic of the broadband transmissive Janus metasurface.

## 2. Metasurface Construction

### 2.1. Metasurface Unit Design

To achieve distinct functionalities under forward and backward incidences, a

broadband polarization conversion unit is designed. The unit cell utilizes a structural combination of split-ring resonators and gratings as shown in **Figure 2**, to achieve orthogonal polarization control for opposite incidence directions. The unit cell comprises dual split-ring resonators, a dielectric layer, and orthogonal top and bottom grating structures. The unit period is 6 mm (approximately $0.3\lambda$, which is less than $0.5\lambda$), the dielectric constant of the substrate is $\varepsilon_r$ = 2.65 with a thickness of 1.5 mm, and the grating layers are employed for polarization selection. The intermediate metallic layer enables polarization conversion at ±45˚, and it consists of two split ring resonators (SRRS) of different sizes to enhance resonance and achieve broadband phase response. By adjusting the opening angle $\psi$ of the SRRS at ±45˚ positions, a continuous phase control of up to 180˚ is achieved. Furthermore, rotating the PB phase by 90˚ enables 360˚ phase coverage. The specific structural parameters are illustrated in **Figure 2**: the radius of the smaller split ring is $r_1$ = 1.1 mm, the radius of the larger split ring is $r_2$ = 2.7 mm, the thickness of both rings is $w$ = 0.6 mm, the opening angle is $\psi$, and the rotation angle of the SRRS is $\phi$. The width of the gratings on the front and back sides is $s$ = 0.6 mm, with a grating spacing of $d$ = 0.6 mm.

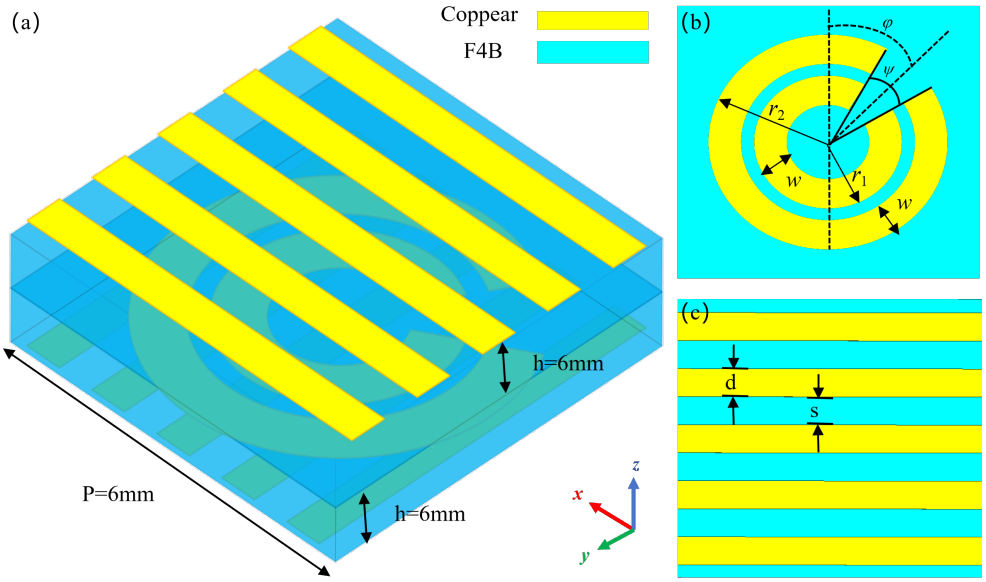


**Figure 2.** Metasurface Unit Structure. (a) 3D structural diagram; (b) Middle-layer SSRS; (c) Front-side grating.

As shown in **Figures 3(a)-(c)**, under forward incidence with x-polarized waves, the optimized unit cell exhibits a linearly continuous variation of phase with the opening angle within the frequency range of 11.35 - 18.6 GHz, easily achieving full 360˚ phase coverage. Within this 48% relative bandwidth, the transmission amplitude remains greater than 0.9, approaching unity. In contrast, under backward incidence with the same x-polarized wave, the transmission drops below –30 dB, nearly total reflection, demonstrating excellent directional selectivity.

As illustrated in **Figure 3(d)**, when the unit cell is illuminated by x-polarized

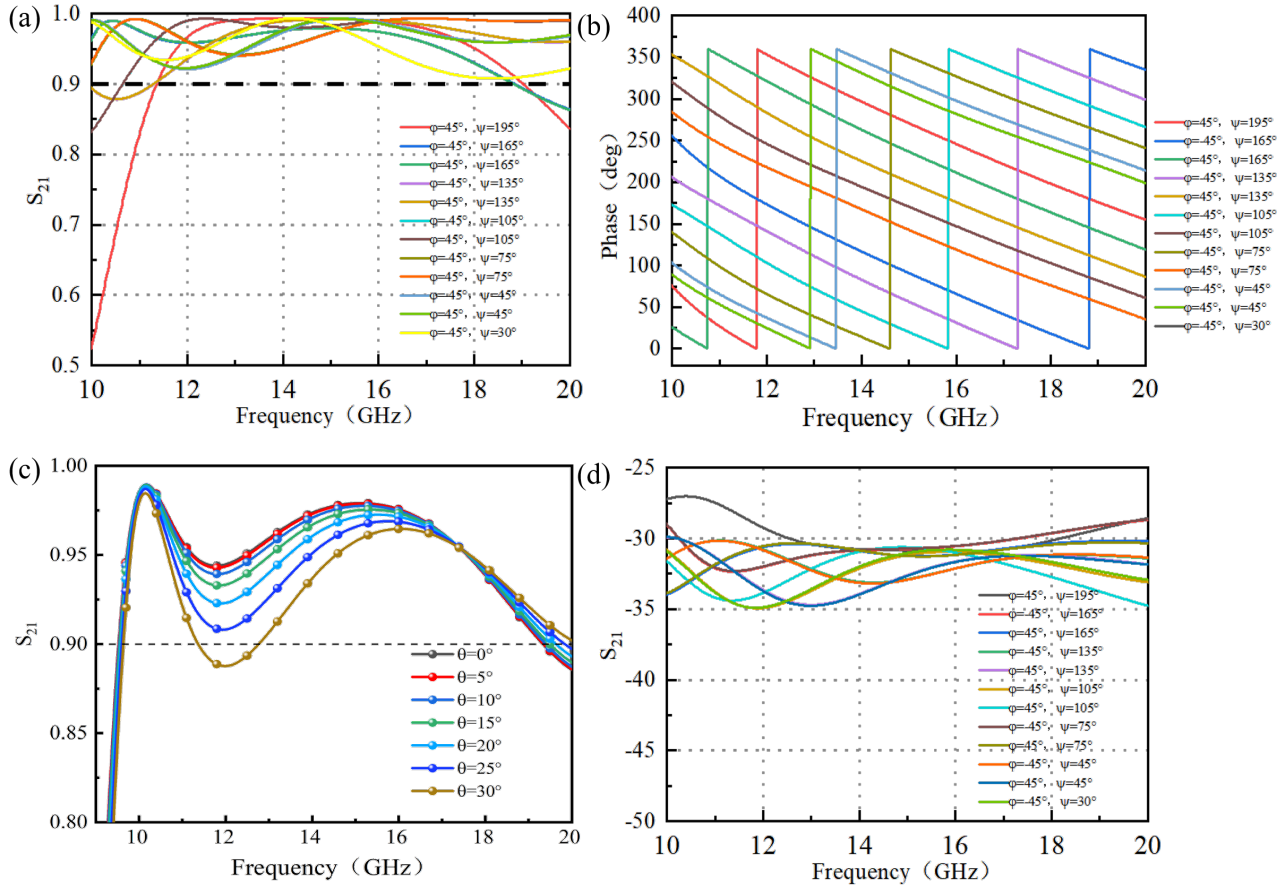


**Figure 3.** Electromagnetic characteristics of the metasurface unit. Under forward x-polarized incidence: (a) amplitude and (b) phase response of the cross-polarized transmission; (c) variation of the amplitude under different incidence angles. Under backward x-polarized incidence: (d) amplitude of the co-polarized transmission.

waves at oblique incidence, its efficiency and operational bandwidth gradually decrease as the incidence angle increases from 0˚ to 30˚ in 5˚ steps. Nonetheless, the efficiency remains above 88.3% even at an incidence angle of 30˚. Therefore, the impact on electromagnetic performance can be considered negligible for incidence angles $\theta$ < 30˚, indicating that the unit cell exhibits good angular insensitivity.

## 2.2. Arrangement and Simulation of Metasurface Arrays

The core of the metasurface array design lies in constructing an interleaved checkerboard topology to achieve independent wavefront control for both forward and backward directions. By deeply coupling two distinct functionalities with their physical arrangement, this design accomplishes complex electromagnetic manipulation within a shared aperture. To improve integration, unit cells are grouped into 2 × 2 supercells to enhance phase performance, with a supercell period of 12 mm. These supercells are then arranged in an interleaved pattern to form a 16 × 16 array. The designed functionalities of the array are as follows: under forward incidence with x-polarization, a beam deflection of 20˚ is achieved; under back-

ward incidence with x-polarization, a vortex beam with a topological charge of 1 is generated. The detailed array phase design proceeds as follows:

First, the phase distributions for beam deflection of unit A and for vortex beam generation of unit B are calculated separately. For beam deflection, according to the generalized Snell's law, to steer the beam to an angle $\theta$, the metasurface needs to introduce a linear phase gradient along the beam-deflection direction:

$$\varphi(x_i) = \frac{2\pi}{\lambda} \cdot d \cdot \sin\theta \cdot x_i \tag{1}$$

where $x_i$ is the position coordinate of the $i$-th element in the array, and $\lambda$ is the operating wavelength. For single-beam deflection, the required target phase for each element is calculated directly according to the above formula, as shown in **Figure 4(a)**.

The vortex phase is calculated based on the orbital angular momentum formula:

$$\varphi = l \cdot \arctan\frac{y}{x} \tag{2}$$

where l is the topological charge order. The transmission phase of each unit in the array is set according to the value calculated from its position (x,y), as illustrated in **Figure 4(b)**.

The two phase profiles are superimposed after removing the phases at the corresponding missing positions in the checkerboard pattern, as shown in **Figure 5(a)**. The units are arranged in an interleaved pattern according to the superimposed phase, with the arrangement of the SRRS array illustrated in **Figure 5(b)**.

Based on the aforementioned design methodology, we conducted full-wave electromagnetic simulations (using CST Microwave Studio) on the fabricated metasurface array to validate its actual performance. When x-polarized waves are incident from the forward direction, the array achieves broadband beam deflection of −30˚, as shown in **Figure 6** and **Figure 7**. At the center frequency of 15 GHz, the deflection angle exactly matches the theoretical value of −30˚. However,

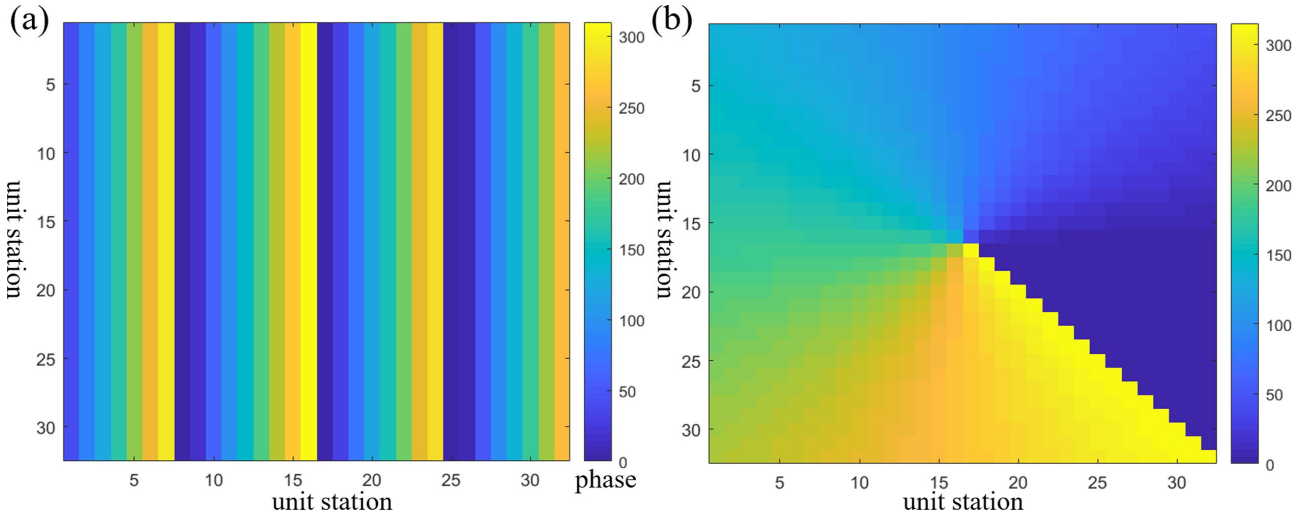


**Figure 4.** (a) 30˚ deflection gradient phase; (b) $l = 1$ vortex phase.

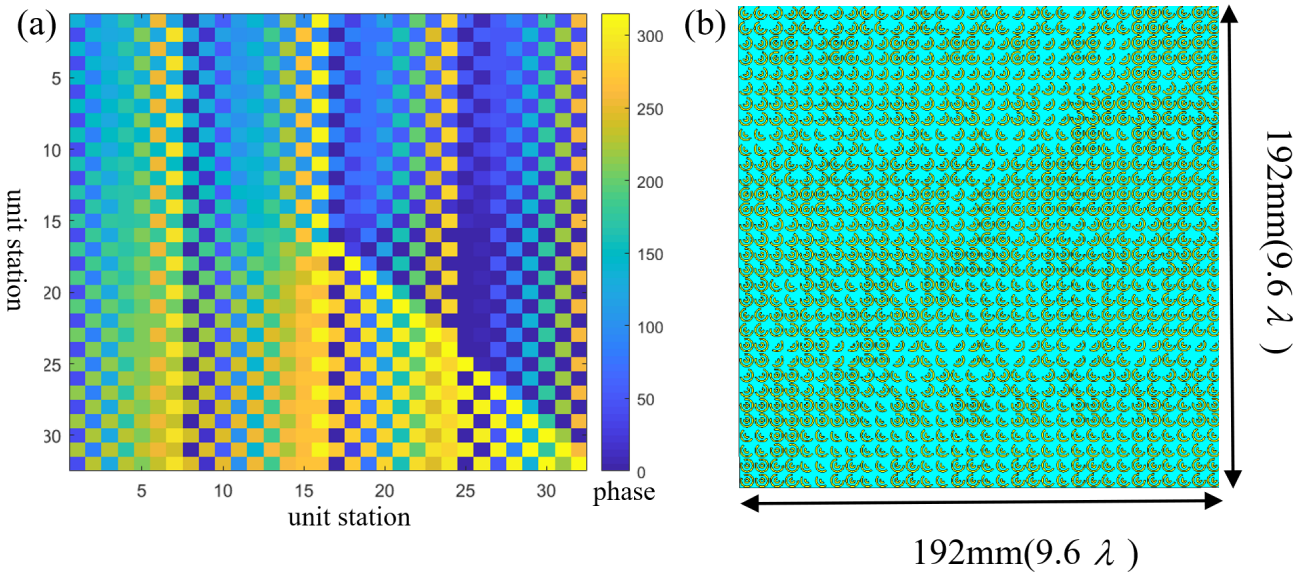


**Figure 5.** (a) Checkerboard superimposed phase; (b)simulated array SRRS distribution diagram.

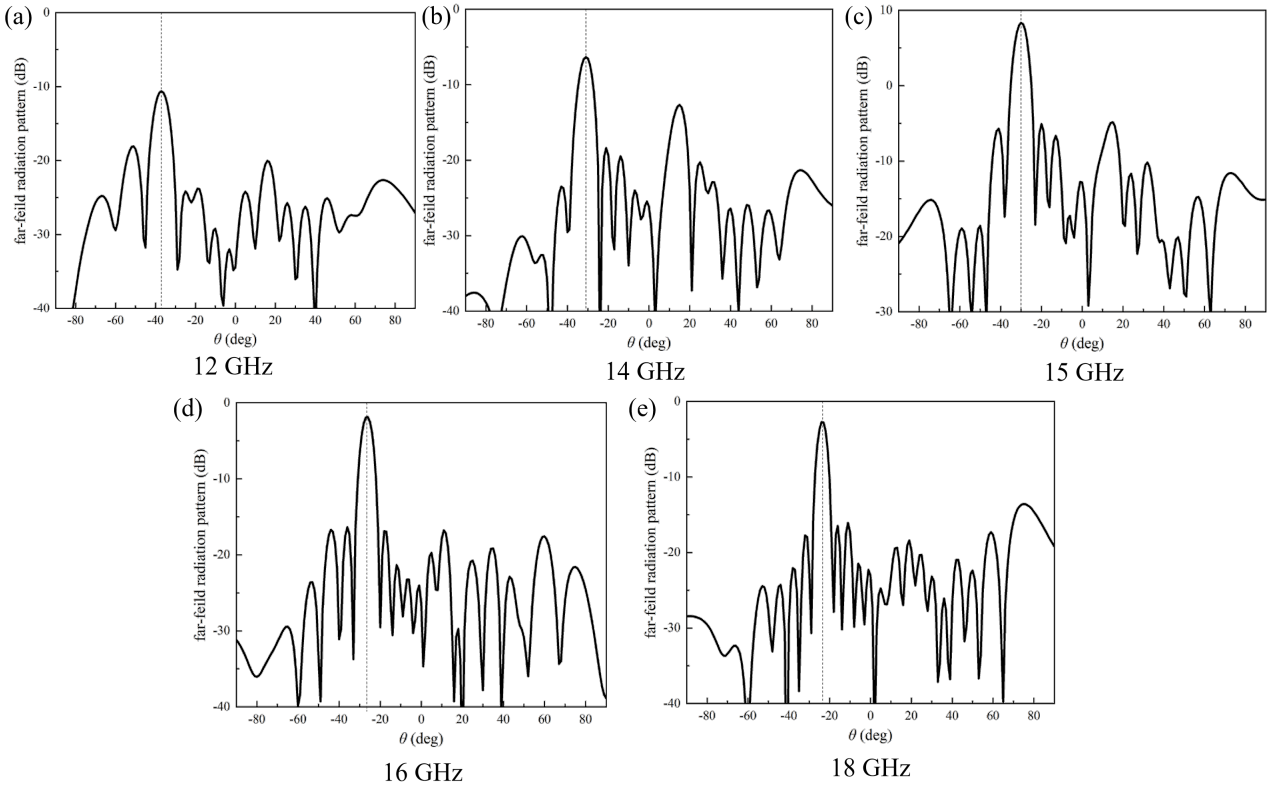


**Figure 6.** One-dimensional far-field scattering patterns of the metasurface array under forward incidence of x-polarized waves in the 12 - 18 GHz frequency band. (a) 12 GHz; (b) 14 GHz; (c) 15 GHz; (d) 16 GHz; (e) 18 GHz.

because the variable $\lambda$ in the formula (1) is frequency-dependent, angular shifts occur at higher and lower frequencies. The farther the target frequency is from the center frequency, the larger the angular error becomes. The simulation results are consistent with the theoretical expectations, and the difference between the main

lobe and side lobes remains above 10 dB, demonstrating good broadband performance.

When x-polarized waves are incident from the reverse direction, a vortex beam with a topological charge of 1 is successfully generated, as shown in **Figure 8** and **Figure 9**. Since the vortex calculation formula is frequency-independent—aside

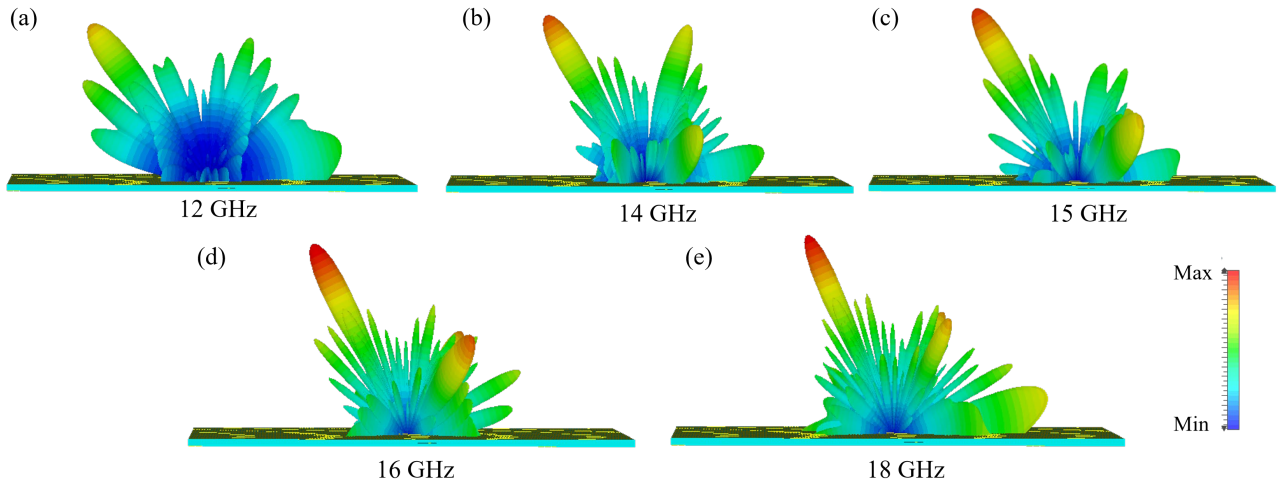


**Figure 7.** Three-dimensional far-field scattering patterns of the metasurface array under forward incidence of x-polarized waves in the 12 - 18 GHz frequency band. (a) 12 GHz; (b) 14 GHz; (c) 15 GHz; (d) 16 GHz; (e) 18 GHz.

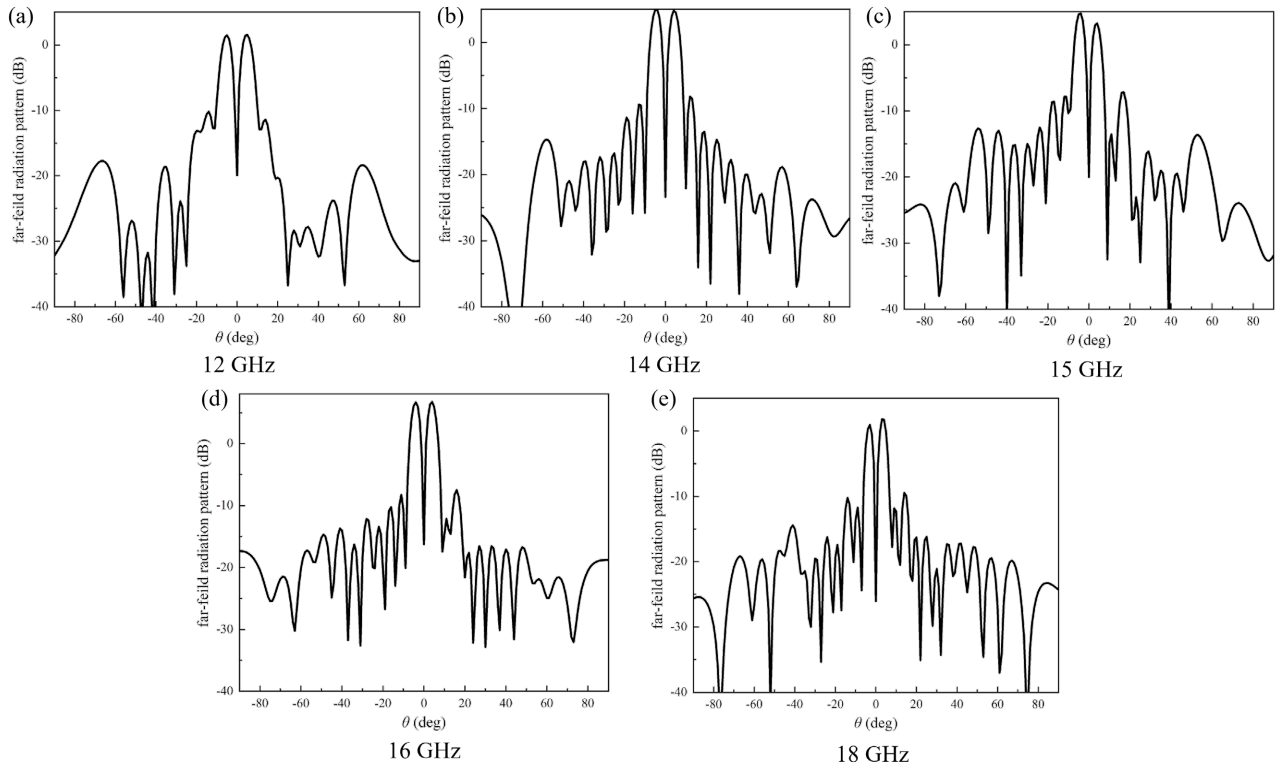


**Figure 8.** One-dimensional far-field scattering patterns of the metasurface array under reverse incidence of x-polarized waves in the 12 - 18 GHz frequency band. (a) 12 GHz; (b) 14 GHz; (c) 15 GHz; (d) 16 GHz; (e) 18 GHz.

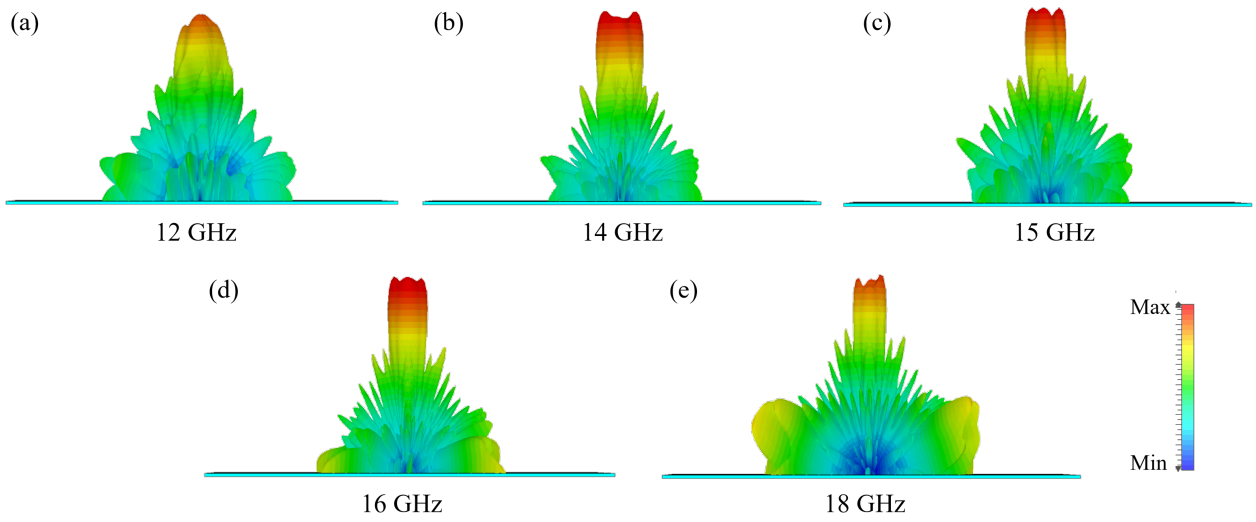


**Figure 9.** Three-dimensional far-field scattering patterns of the metasurface array under backward incidence of x-polarized waves in the 12 - 18 GHz frequency band. (a) 12 GHz; (b) 14 GHz; (c) 15 GHz; (d) 16 GHz; (e) 18 GHz.

from minor variations in the phase relationship of the units at different frequencies—the vortex effect is maintained across the entire broadband, verifying the broadband performance of the array and confirming the independent control capability between the forward and backward channels.

## 3. Conclusion

This study successfully designed and validated a broadband transmissive Janus metasurface. Through the design of a broadband polarization conversion unit and a checkerboard interleaved arrangement, asymmetric transmission and independent wavefront control under forward and backward incidences within a broadband range were achieved. Within a 40% bandwidth, the metasurface realizes −30˚ beam deflection under forward incidence and generates a vortex beam with a topological charge of 1 under backward incidence. Simulation results validate the feasibility and broadband performance of the design. Future work can be extended to dynamic reconfigurable designs, applications in higher frequency bands, as well as experimental fabrication and testing, promoting the practical development of this type of metasurface.

## Conflicts of Interest

The authors declare no conflicts of interest regarding the publication of this paper.

## References

[1] Bai, X., Zhang, F., Sun, L., Cao, A., Wang, X., Kong, F., *et al.* (2022) Radiation-Type Programmable Metasurface for Direct Manipulation of Electromagnetic Emission. *Laser & Photonics Reviews*, **16**, Article 2200140. https://doi.org/10.1002/lpor.202200140

[2] Liu, T., Wang, Y., Feng, W., Luo, H., Wang, Z., Wang, H., *et al.* (2025) Synergetic Full-Parametric Aharonov-Anandan and Pancharatnam-Berry Phase for Arbitrary Polarization and Wavefront Control. *Nanophotonics*, **14**, 3657-3667. https://doi.org/10.1515/nanoph-2025-0357

[3] Wang, Y., Luo, H., Shao, Y., Wang, H., Liu, T., Wang, Z., *et al.* (2024) Detection and Anti-Detection with Microwave-Infrared Compatible Camouflage Using Asymmetric Composite Metasurface. *Advanced Science*, **11**, Article 2410364. https://doi.org/10.1002/advs.202410364

[4] Xu, H.X., Hu, G., Wang, Y., Wang, C., Wang, M., Wang, S., *et al.* (2021) Polarization-insensitive 3D Conformal-Skin Metasurface Cloak. *Light*: *Science & Applications*, **10**, Article No. 75. https://doi.org/10.1038/s41377-021-00507-8

[5] Xu, H.X., Wang, Y., Wang, C., Wang, M., Wang, S., Ding, F., *et al.* (2021) Deterministic Approach to Achieve Full-Polarization Cloak. *Research*, **2021**, 1-13. https://doi.org/10.34133/2021/6382172

[6] Mu, Y., Xia, D., Han, J., Ma, X., Wang, X., Liu, H., *et al.* (2024) Time-Space-Coding Radiation-Stealth Metasurface with Amplitude-Phase Co-Modulation. *Advanced Functional Materials*, **34**, Article 2407802. https://doi.org/10.1002/adfm.202407802

[7] Shang, G., Li, G., Zhao, W., Zhang, K., Wu, Q., Liu, J., *et al.* (2024) Interleaved Coding Janus Metasurface with Independent Transmission and Reflection Phase Modulation. *Optics Express*, **32**, Article 1451.

[8] Chen, K., Ding, G., Hu, G., Jin, Z., Zhao, J., Feng, Y., *et al.* (2019) Directional Janus Metasurface. *Advanced Materials*, **32**, Article 1906352. https://doi.org/10.1002/adma.201906352

[9] Yang, W., Chen, K., Dong, S., Wang, S., Qu, K., Jiang, T., *et al.* (2023) Direction-duplex Janus Metasurface for Full-Space Electromagnetic Wave Manipulation and Holography. *ACS Applied Materials & Interfaces*, **15**, 27380-27390. https://doi.org/10.1021/acsami.3c04382